Copepod Aggregations: Influences of Physics and Collective Behavior

Glenn R. Flierl · Nicholas W. Woods

Abstract Dense copepod aggregations form in Massachusetts Bay and provide an important resource for right whales. We re-examine the processes which might account for the high concentrations, investigating both horizontally convergent flow, which can increase the density of depth-keeping organisms, and social behavior. We argue that the two act in concert: social behavior creates small dense patches (on the scale of a few sensing radii); physical stirring brings them together so that they merge into aggregations with larger scales; it also moves them into areas of physical convergence which retain the increasingly large patch. But the turbulence can also break this apart, suggesting that the overall high density in the convergence zone will not be uniform but will instead be composed of multiple transient patches (which are still much larger than the sensing scale).

Keywords Biological-physical aggregation · Social behavior · Horizontally convergent flow · Plumes

1 Introduction

Aggregation of prey in the ocean plays a vital role in food web ecology. Some predators may not be able to survive without prey aggregation. For example, sea lions, killer whales, and sea birds feed on schools of herring [20,22], blue whales feed on swarms of krill [25], and basking sharks, cod, haddock, and right and sei whales feed on highly concentrated patches of copepods [26–28]. The processes that aggregate prey therefore play an important part in fisheries management and species conservation.

G. R. Flierl (✉)
Department of Earth, Atmospheric, and Planetary Sciences, Massachusetts Institute of Technology, Cambridge, MA 02139-4307, USA
e-mail: glenn@lake.mit.edu

N. W. Woods
CNA Corporation, 3003 Washington Blvd, Arlington, VA 22201, USA

Fluid flow in the ocean is effectively incompressible, and so true water-following particles will never aggregate. However prey in the ocean may differ from a true Lagrangian particle by swimming, and this may result in the formation of patches. As an example, the role of convergent fronts in aggregating zooplankton has been the focus of several different studies [10,13, 15,19]. While the details of each investigation differ, the main message is consistent between them: as neutrally buoyant or actively swimming organisms are swept towards a convergent front, the concentration of organisms will increase at the front as the flow sinks and the organisms are left behind (either by actively swimming or being constrained to a depth surface).

In the Gulf of Maine (GOM), in particular, aggregations of copepods play an important role in the ecosystem. These aggregations are a food source for many species, including the endangered right whales (*Eubalena glacialis*), which return to the southwestern GOM every spring to forage. Past experiments have suggested that the interaction of biological and physical processes may create these dense aggregations. The South Channel Ocean Productivity Experiment ("SCOPEX", [28]) noted that the location of the densest patches occurred within a general area of high copepod abundance, which appeared to coincide with the salinity front on the eastern edge of the Channel. From net-tows, the densest patches were found to range in size from 100–1,000 m across, while the vertical extent of these patches is in the range of 1–10 m [3,28]. Observations of peak density within a patch are in the range of 10^3–10^4 copepods/m^3 ([4,28]), which is one to three orders-of-magnitude larger than typical values measured in the GOM in spring-time [2,28]. The temporal persistence of the patches is somewhere between hours and days; however, what determines this time scale is unknown (M. Baumgartner, pers. comm.). Since SCOPEX, the leading hypothesis to explain high concentrations of copepods found in patches in the southwestern GOM has been that advection by circulation and coupled physical-biological mechanisms were likely to be aggregating copepods. The SCOPEX team ruled out in situ growth and social behavior as likely causes for the observed high-concentration patches in the southwestern GOM. The physical side, however, was not ruled out, and in fact some evidence for a coupled physical-biological aggregating mechanism was observed [10,13].

We will re-assess the physical aggregation mechanisms and argue that the time-dependent development, both downstream and in association with eddies, makes the physical convergence much less likely to increase the concentration to the levels observed (Sect. 2). At the same time, social mechanisms may give large densities, but are not likely to create patches on the scales of kilometers (Sect. 3). Therefore, we propose a multi-stage process for the development of large, high-density aggregations (Sect. 4): (a) social behavior leads to high-density but small-scale patches; (b) turbulent flow brings patches in contact where they can stick together; (c) weak convergence accumulates the patches and they coagulate into larger regions of elevated concentration which, because of the social behavior, are able to resist (to some degree) being sheared apart.

2 Concentration of Depth-Keeping Organisms by Fluid Flow

We begin by reviewing the role of directed vertical swimming which allows us to treat the concentration as governed by a two dimensional (horizontal) flow which is divergent or convergent. We discuss briefly examples of steady flows analogous to those used in previous treatments (e.g. [9,13]), before moving to time-dependent flows and to more realistic simulations relevant to the flows in the GOM.

The three-dimensional flow in the ocean is effectively incompressible so that the concentration of passive tracers will not be increased by advection. But copepods, like many ocean

organisms, can swim vertically much more rapidly than the fluid moves. To derive density equations with this included, we shall deal with two descriptions, one based on the density (number per unit volume) of organisms $b(\mathbf{x}, z, t)$ and one on the positions of individuals $\mathbf{X}_i(t)$, $Z_i(t)$. Vectors will be used for horizontal coordinates and velocities; the vertical terms will be written explicitly.

If we treat the organism positions stochastically, and their movements are independent, the probability of being in a small volume around some point $P(\mathbf{x}, z, t)dV$ satisfies an advection-diffusion equation like that for density. This relies on the mean free path being short compared to scales over which the fluid velocities or swimming properties vary significantly; that may not strictly be true (e.g., the organisms could be executing Lèvy flights) but, given our lack of knowledge about the swimming behavior, it seems to be a reasonable starting point. Therefore, we shall begin by examining the density equation.

The concentration $b(\mathbf{x}, z, t)$ of organisms satisfies

$$\frac{\partial}{\partial t}b + \nabla_i(U_i b - K_{ij}\nabla_j b) = 0$$

where the three component velocity U_i and the diffusivity K_{ij} include both fluid motions and swimming. If we integrate this equation over a small volume around a local maximum, the diffusive fluxes will be negative, while those from the fluid flow will be zero (since it is non-divergent in 3D). The only term, then, that can increase the concentration is convergence of the swimming velocity.

We want to take advantage of the fact that, for zooplankton, vertical swimming can be significant compared to fluid velocities and length scales, whereas horizontal movements are dominated by the flow. Previous papers have applied this idea, (e.g. [5,6,9,13,19]) but have focused more on analytical x–z flows whereas we are interested in flows with complex horizontal structure. As Appendix 1 shows, if the vertical swimming and its random variability overcome the fluid motions and cause clustering around the preferred depth, the biomass density can be represented as $\tilde{b}(\mathbf{x}, t)F(z)$ where

$$\frac{\partial}{\partial t}\tilde{b} + \nabla \cdot (\tilde{\mathbf{u}}\tilde{b} - \tilde{K}\nabla\tilde{b}) = 0, \quad \tilde{\mathbf{u}} = \int dz\, F\mathbf{u}, \quad \tilde{K} = \int dz\, F K$$

and $F(z)$ has been normalized by $\int dz\, F = 1$, making $\tilde{b}$ the column-integrated biomass. But the horizontal velocity $\tilde{\mathbf{u}}$ is not non-divergent; indeed

$$\nabla \cdot \tilde{\mathbf{u}} = \nabla \cdot \int F\mathbf{u} = \int F\nabla \cdot \mathbf{u} = -\int F\frac{\partial w}{\partial z} \equiv -s$$

where the "stretching" s will determine whether the flows are causing increases in concentration ($s > 0$) or decreases ($s < 0$).

The resulting equations look the same as those obtained by assuming the organisms occupy a 2D surface and compensate completely for the vertical motions (corresponding to a delta function for $F(z)$); however, the advecting velocities and stretching are smoothed versions over the depth range occupied by the copepods. We shall drop the tildes and analyze

$$\frac{\partial}{\partial t}b + \nabla \cdot (\mathbf{u}b - K\nabla b) = 0 \tag{1a}$$

or

$$\frac{\partial}{\partial t}b + \mathbf{u} \cdot \nabla b - \nabla \cdot K\nabla b = sb, \quad s = -\nabla \cdot \mathbf{u} \tag{1b}$$

We can also decompose the velocity into a rotational and divergent part

$$\mathbf{u} = \mathbf{u}_\psi - \nabla\phi, \quad \mathbf{u}_\psi = \hat{\mathbf{z}} \times \nabla\psi$$

The $\mathbf{u}_\psi$ will not cause increases in density. When we include social movement, we will add functionals of b to ϕ or K, but assume that this part of the motion does not have a rotational component. Most of the results in the next section, therefore, will be easy to rephrase for the case with behavior.

2.1 Steady State Patches

If the flow is steady (which could involve a Galilean reference frame shift), the patches will also be steady if the flux

$$\mathbf{F} = \mathbf{u}b - K\nabla b$$

is non-divergent; i.e., $\mathbf{F}$ is the curl of some vector field $\mathbf{F} = -\nabla \times [\hat{\mathbf{z}}\chi(\mathbf{x})] = \hat{\mathbf{z}} \times \nabla\chi$. Since the divergence of the flux creates the enhancement of patch density, we can understand the dynamics of patch formation below by neglecting, for the moment, χ and $\mathbf{u}_\psi$ and looking at the solution of

$$-b\nabla\phi - K\nabla b = 0 \quad \text{or} \quad \nabla \ln b = -\frac{1}{K}\nabla\phi$$

which, in the constant K case, yields

$$b = b_0 \exp(-\phi/K) \tag{2a}$$

Concentrations peak at the minimum points of ϕ where the convergence is largest, but are less pronounced when the diffusivity is high. If contours of K are parallel to those of ϕ, we can find a similar solution

$$b = b_0 \exp\left(-\int d\phi \frac{1}{K(\phi)}\right) \tag{2b}$$

which has much the same character. In the following examples, we shall use constant K for simplicity.

The forms (2) show that the solutions depend on one non-dimensional parameter, the Péclet number $P = UL/K$, which measures the strength of advection by the divergent flow ($U \sim |\delta\phi|/L$) to diffusion. We shall continue to write the equations in dimensional form, but illustrate results in non-dimensional form by choosing $U = 1$, $L = 1$, and $K = 1/P$.

When the flow is independent of one direction (e.g. y or θ for a circularly symmetric case—see Appendix 2), b can also be one-dimensional if the boundary conditions allow it. In that case, the component of the flux in the direction of variation must be constant (zero for the circular geometry because of conditions at $r = 0$). Table 1 and Fig. 1 describe the three basic cases for rectilinear flows. More details are in the appendix; here we simply note that the commonly used profiles with flows extending far from the front (pure strain and localized convergence) have steady states with a finite total population and concentrations which decay rapidly away from the center of the convergence. In contrast, when the flow decays away from the front, the far-field concentration is non-zero but b still has a peak with amplitude e^P higher than the background at the front. In the other cases, the peak concentration depends on the total population, which really means the size of the area from which the copepods in the front are drawn. As an example, if we have localized convergence acting on copepods distributed

Table 1 Flows and densities

Description	Flow/density	Potential
1. Pure strain	$u = -Ux/L$	$\phi = \frac{1}{2}(x/L)^2$
	$b = b_0 \exp\left(-\frac{1}{2}P(x/L)^2\right)$	
2. Localized conv.	$u = U_0 - U\tanh(x/L)$	$\phi = -U_0 x + UL\ln[\cosh(x/L)]$
	$b = b_0 \exp(P_0 x/L)\mathrm{sech}^P(x/L)$	
3. Localized u	$u = -(x/L)\exp\left(-\frac{1}{2}(x/L)^2\right)$	$\phi = -UL\exp\left(-\frac{1}{2}(x/L)^2\right)$
	$b = b_0 \exp\left(Pe^{-\frac{1}{2}(x/L)^2}\right)$	

uniformly over an width L_{init}, the final peak value will be about $b_{\mathrm{init}}(L_{\mathrm{init}}/L)\sqrt{P/2\pi}$. Given time and a large reservoir, the density can increase dramatically.

These large concentrations seem to justify the previous arguments that the physical convergence dominates. However, they do not take into account the possibility of advective losses (e.g., sideways), the time-dependence of the convergent flow, or turbulence on the frontal scale which can transport the organisms away from the front.

2.2 Physical Effects in Mass Bay

In this section, we will discuss models of one of the potentially significant flows causing concentration increases in the Great South Channel. Lateral convergence may be found at density fronts such as those at the nose of a buoyant plume. In the spring in the GOM, buoyant plumes form as a result of increased river discharge, and are often observed to propagate down the coast [12]. Woods [29] analyzed lateral convergence in a realistic numerical model of the GOM circulation and noted a period of enhanced convergence associated with buoyant plume events (see Fig. 2). The stretching $\frac{\partial w}{\partial z}$ corresponds to increasing the concentration by a factor of 2 per day, but is clearly unsteady. In addition, the plume has a two-dimensional structure, extending from the coast to order 5 km offshore, and there are flows relative to the moving plume within the freshwater (c.f., [16]). Thus, organisms can be carried away from the front, rather than continue to accumulate.

Although there is large convergence at the plume front (Fig. 2), the $x-y$ structure indeed ends up limiting the enhancement of the density. In Appendix 4, we present a number of simple examples which illustrate different aspects of the dynamics; here, we consider a curved front such as that shown in Fig. 3, where there is convergence at the front as it moves through still fluid (which is pushed down underneath it, leaving the copepods in the surface layer) as well as some front-relative circulation that redistributes them within the plume. The front in this model is steadily advancing (from left to right in Fig. 3, with the velocity arrows shown in the reference frame moving with the plume) at a speed c, and the front-relative circulation is given by

$$\psi = \begin{cases} u_0\, y\, [y + \tanh(2x)] & y < -\tanh(2x) \\ cy & x > 0 \text{ or } y > -\tanh(2x) \end{cases}$$

Since the major "convergence" here is the plume running into still water, the maximum possible number of organisms in the front depends on the area swept out by the plume; this increases linearly with t. The buildup will continue until the input is balanced by advective losses. In the
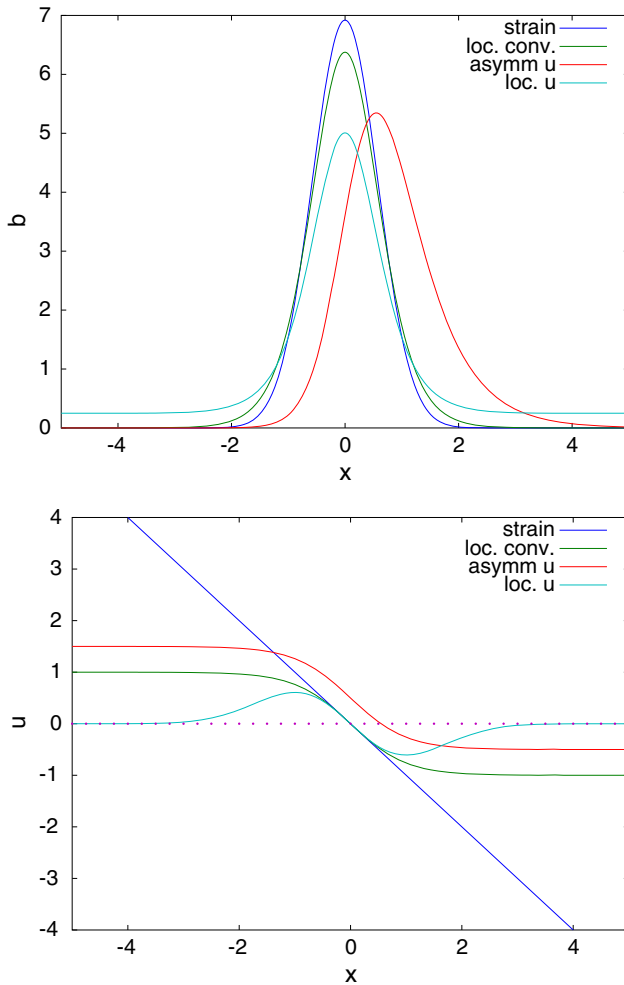
Fig. 1 Solutions for pure strain (*blue*), localized convergence with symmetric inflow in the far field (*green*), localized convergence with stronger inflow on the *left* ($U_0/U = P_0/P = 0.5$, *red*), and localized velocity field (*cyan*). $P = 3$ is deliberately small to show the structure, and the densities have been normalized to have average value 1. For reference, the maximum is 20 times the background for the localized velocity case (and 2.2×10^4 when $P = 10$). Velocity fields are shown below (Color figure online)

case $u_0 > 0$, the relative flow converges at the nose but diverges out along the front. In contrast, when $u_0 < 0$, the flow relative to the nose pushes the offshore organisms in towards the corner, enhancing the concentration until diffusion and advective losses along the wall can balance the incoming flux. Since the patch is more confined, the concentrations tend to be higher. When there is no relative flow in the plume ($u_0 = 0$), the influx is only lost to a lengthening diffusive plume in the quiescent region behind the nose, and the amplitude grows roughly as $t^{1/2}$.

We can estimate the maximum concentration by noting that the flux $\mathbf{F}$ tends towards a constant. If $|u|$ decreases monotonically along a trajectory, but does not become zero, the maximum will be reached in the outflow region $b_{\max} = b_{\text{in}} u_{\text{in}} / u_{\text{out}}$. If u decreases to zero and then increases again, the flux will be carried by diffusion through this low velocity region of width ℓ so that $F \sim -K(b_{\max} - b_{\text{out}})/\ell = u_{\text{in}} b_{\text{in}} = u_{\text{out}} b_{\text{out}}$ giving
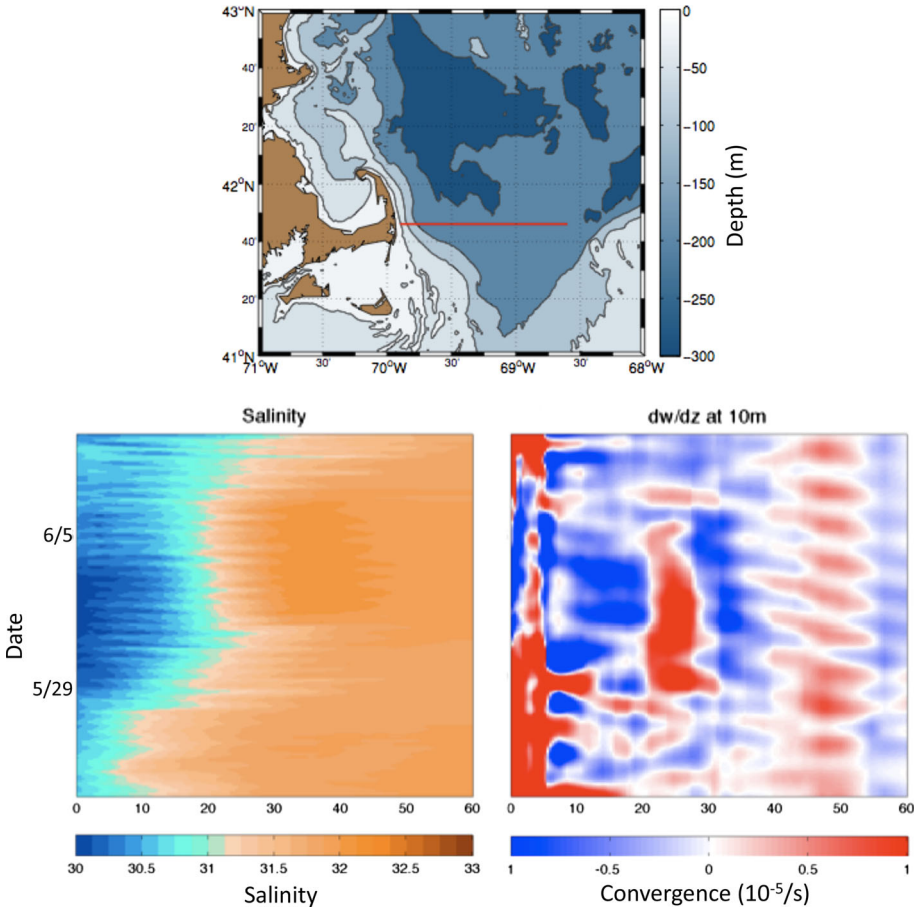
Fig. 2 FVCOM simulations showing enhanced convergence at the outer edge of a buoyant plume (low salinity water) passing Cape Cod. *Upper panel* shows the section. The *lower panels* show the salinity (*left*) and stretching $\frac{\partial w}{\partial z}$ (*right*) as functions of distance along the track and time increasing from *bottom to top* over about 2 weeks. A plume of freshwater crosses the section beginning on May 29. For the week following the start of the event, convergence can be found just offshore of the plume (near 25 km from shore). See Woods [29] for details

$b_{max}/b_{in} = (u_{in}/u_{out}) + (u_{in}\ell/K)$, which grows only linearly with the Péclet number. This picture—the organisms pile up as the flow velocity drops until the diffusive flux is able to carry them across into the outflow—is reasonable for $u_0 \neq 0$. When there is no plume-relative flow inside ($u_0 = 0$), the density builds up at the front, with diffusion spreading the organisms into the plume. The diffusive tail decays over a scale $\ell = \sqrt{Kt}$ and has order $b_{max}\ell$ organisms; equating this to the number swept up by the movement, $u_{in}b_{in}t$ gives $b_{max} \sim t^{1/2}$.

The quantitative difference between the experiments with front-relative flow and the 1D model in Sect. 2.1 (and previous models such as [10] or [14]) is significant: when the organisms can be swept away by the plume-relative flow, the amplitude will not build up nearly as much.

As the complexity of the model increases towards that of reality, different behavior with time of the maximum b is observed. Woods [29] examined the concentration using several
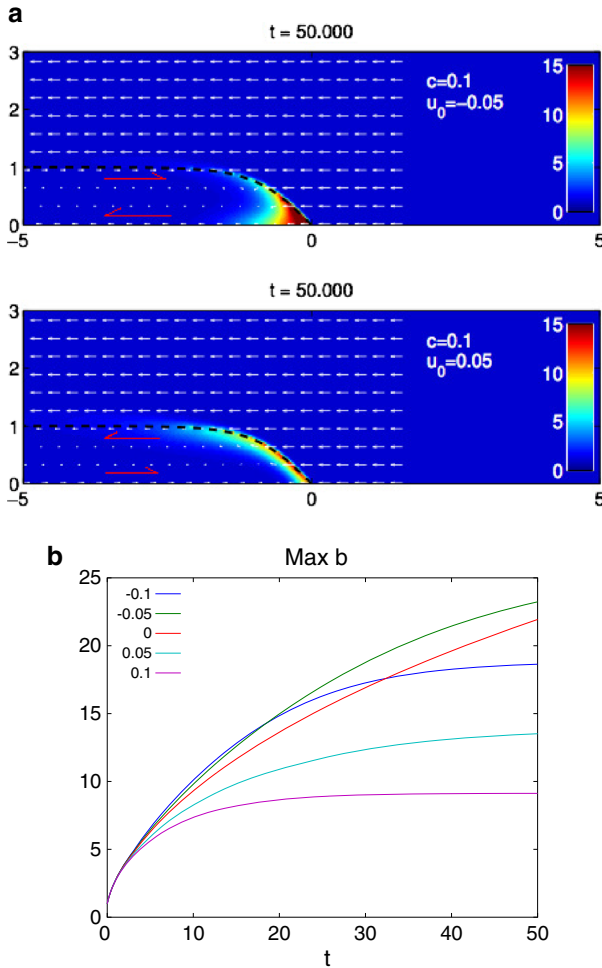
Fig. 3 a Examples of the density of a depth-keeping organism in a front moving from left to right at speed 0.1 with the flow behind the front moving towards or away at a front-relative speed ± 0.05. $K = 8 \times 10^{-4}$. The plots are in the reference frame of the nose of the front, so the *arrows* show motion relative to the front. The *color scale* is b with the background value being 1. **b** Maximum concentration for different values of the inflow along the wall, $u_0 = -0.05, 0, -0.1, 0.05, 0.1$ (in order from the top for $t = 50$). One non-dimensional time unit would correspond to about 0.25 d (Color figure online)

dynamical models of buoyant plume (ROMS and a 2.5 layer model); these gave amplification factors over 5 days of order 4 compared to the model above which gives order 10–20; however, the front model with fixed structure above (the "plow", as in a snowplow with material swept into a pile which eventually escapes around the sides) can be adjusted to give a similar amplification (Fig. 4). This difference probably can be attributed to more complex circulations, especially near the nose, but also to the fact that the plume slows down and therefore gathers up fewer and fewer organisms in a given amount of time.

A slowing plume is a simple form of time-dependence, one for which it seems clear that the growth rate will decrease as the convergence is reduced. However there are many other sources of variability in the GOM which may also make the physics less able to create
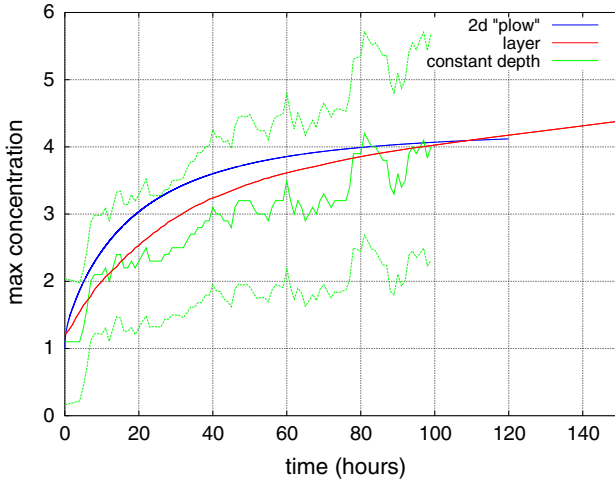
Fig. 4 Comparison of the simple 2D model (labeled "2d plow") to dynamical models of idealized plumes. The parameters are $c = 0.14$ m/s, width 5.2 km, $K = 10^6$ m^2/s, $u_0 = -0.3c$. The width of the nose (in the tanh function) is the same as the plume width. The *red curve* shows the 2.5 layer model, and the center *green curve* show the mean concentration of a set of depth-keeping particles in the ROMS simulation. The outer *green curves* show one standard deviation (Color figure online)

and maintain dense patches. Equation (1) has some obvious time scales: convergence L/U, diffusive L^2/K, and, for flows extending far from the front, similar scales involving the size of the region from which the organisms can be gathered. But there are more subtle time scales as well: that for shear dispersion along streamlines ψ and for chaotic mixing, both of which may again limit increases in b. Solutions which continue to grow (e.g. the $t^{1/2}$ case above) as organisms are continually brought into the convergent region may not be very relevant to the ocean: we cannot expect the flows to remain steady over many diffusion time-scales. Instead, the large convergences are associated with eddies and transient events such as intrusion of freshwater plumes along the coast in the spring as the river runoff peaks. As an example, [29] examined the expected enhancement of b following simulated trajectories: from

$$\frac{D}{Dt} \ln b = s$$

the growth would be

$$\ln \left[\frac{b(t)}{b(0)} \right] = \int_0^t s$$

where the integral is taken along a Lagrangian trajectory. In an Eulerian frame, the convergence can be quite large: that predicted by a full Gulf of Maine model reaches a factor of 7 per day but varies significantly from point to point (c.f. southern part of GOM in Fig. 5). But fluid parcels (and copepod patches) do not generally stay for long periods in one of these regions of convergence (such as that north of Cape Cod which shows high positive values of $s = \frac{\partial}{\partial z} w$), and s also has significant temporal variability. Figure 5 shows that the integrated value of s following fluid parcels at 10m, which gives the change in $\ln b$. It can be quite large for a few simulated drifters (a growth by a factor of order $e^5 = 150$, but, in most cases, it gives at best a modest increase (order 2–5). Nor is there a consistent pattern suggesting large increases for points ending up in the Great South Channel. Finally, we note that vertical

a

b
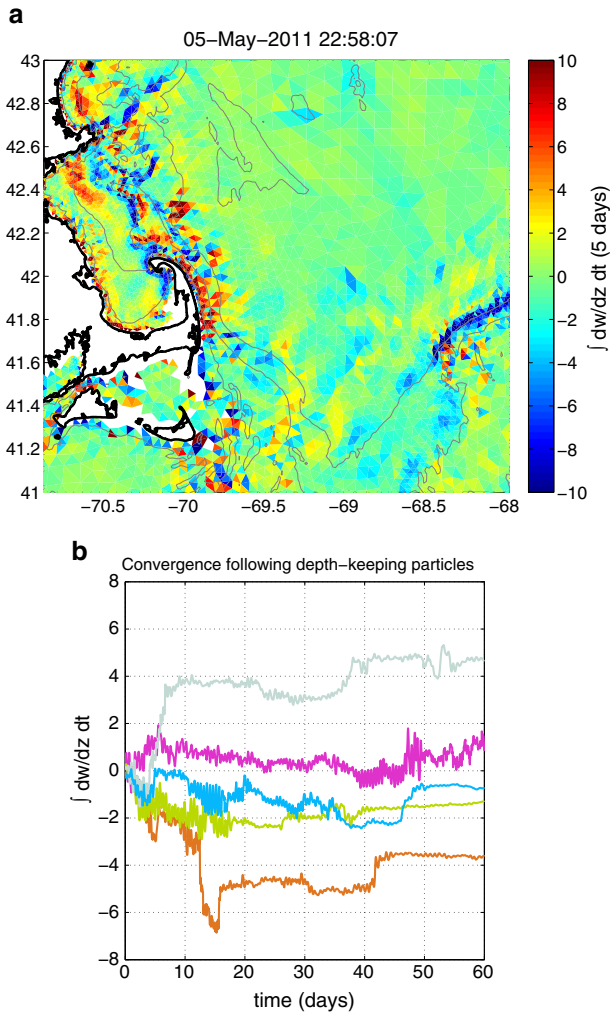
Fig. 5 a Distribution of the de-tided stretching ($\int_0^{5d} \frac{\partial w}{\partial z}$) values in the FVCOM model [7]. **b** Value of the integral of the stretching along several trajectories which pass through or close to the Great South Channel

velocities in hydrostatic models are often noisy (as indicated by the large variation from cell to cell in Fig. 5); the detailed high resolution frontal models (Fig. 4) have smoother w's and do not give very large numbers.

These results indicate that the analytical model predictions of large enhancements [order $\exp(P)$] rely heavily on the horizontal convergence being stable and persisting for long enough to gather copepods from large distances and concentrate them in a small area. But consideration of the time-dependence indicates these concentrations would take far longer to build up than is reasonable given the levels of variability in the currents. Experiments with two-dimensional (in the horizontal) flows, with plumes having realistic dynamics, and with the GOM FVCOM model also suggest that the 1D calculations overestimate the likely concentrations: fluid parcels do not stay in regions of strong convergence for long enough

times. As we shall see, stirring by eddies (which can be thought of as greatly reducing P) also limits the concentration.

3 Social Behavior

The results above suggest that we should consider factors beyond the physics: the convergence in realistic plume models is not large enough to magnify the concentration by several orders of magnitude; the vertical velocities in the full GOM model are spatially and temporally quite variable, so that only a few trajectories show strong amplification. We now turn to examining how social behavior might contribute, and, especially, how it can combine with the fluid flow. Social behavior can lead to patchiness either by directed swimming where organisms move towards others or, more passively, by a reduction in the random swimming. As [11] point out, both of these appear as convergent motions either $\mathbf{u}_b[b] = -\nabla \phi_b[b]$ or $-\nabla K_b[b]$ where the brackets indicate the biological swimming or diffusion are functionals of the density b, meaning in this case that the value at a point $\mathbf{x}$ will depend on the density in a neighborhood of $\mathbf{x}$ (see explicit examples below). The size of this neighborhood is order of the sensing distance; however, we hope (and will see) that the patches can be considerably larger. If ϕ_b or K_b is low where the density is high, organisms will converge into that region, leading to further density increases. The two cases—called "social taxis" and "social kinesis"—are similar in this respect but differ because the spatial/temporal variations of K_b in the latter affect not only the convergence but also the diffusive spreading.

Desirable features of the social grouping model we shall consider include:

– Spontaneous break-out of patchiness. Not surprisingly, this tends to occur at the sensing scale.
– Shear resistant. Patches should be maintained under reasonable shear or strain in the fluid flow.
– Sticky. If two patches are brought near enough by the eddies or other motions, they should coalesce to form a larger patch which can hold together.
– Potential for large-scale, stable patches. If patches begin to coagulate, but then break down again, dense aggregations on a scale much bigger than the sensing scale are unlikely.

The combination of these features seems to be critical for the development of large-scale, dense aggregations like those seen in the Great South Channel. Social aggregation can cause a uniform region to develop lots of small patches, but, even though the density on the centimeter scale might be very high, the average over larger scales is not altered since the patch is drawing from the local neighborhood. Physical convergence acts on these just as on independent particles, so that the smoothed concentration will grow as in the previous section, but does not get very high. On the other hand, horizontal turbulence (mostly in the ψ term) can bring patches into contact (c.f., the work on encounter rates in turbulence such as [24]). If they merge into a larger patch which is still able to resist being torn apart by shear so that the organisms do not depart as the water moves away, the smoothed density will increase with each coagulation. But if these large patches are unstable to formation of small aggregations within themselves, they will break up again and become vulnerable to being dispersed by the flow.

3.1 A Social Aggregation Model

We now describe a model for movement which will prove to have the characteristics above and which seems to make some biological sense. Taxis, rather than kinesis, will be used both

because it makes analysis more straightforward but also the resulting patches are generally more robust. We represent the movement as random accelerations balanced by relaxation back to a preferred swimming velocity which depends on the flow and the distribution of neighbors. For the nth organism,

$$dX^{(n)} = V^{(n)}dt$$
$$dV^{(n)} = -r(V^{(n)} - u - u_b)dt + dW \tag{3}$$

with dW a random increment (different for each organism) satisfying $\langle dW \rangle = 0$ and $\langle dW_i dW_j \rangle = 2K_b r^2 dt\, \delta_{ij}$ with subscripts indicating vector components. Here u_b is the preferred swimming velocity (a functional of b), and K_b is the biological diffusivity associated with the random component of the swimming. In the absence of fluid flow and a preferred velocity, the individuals all move independently, their velocity variance stabilizes, $\langle V_i V_j \rangle \to r K_b \delta_{ij}$, and the mean square displacement grows with time $\langle X_i X_j \rangle \to 2K_b t\, \delta_{ij}$ exactly as produced by diffusion with diffusivity K_b (thus the choice of normalization for the random increment).

As mentioned, we take K_b to be a constant which includes the effects of fluid turbulence at the scale of the copepod (or Brownian motion for smaller creatures) and random swimming which can be a sizable contribution. The social behavior is manifested in u_b. The social taxis model assumes that the organisms can perceive a rough measure of local density and which directions have higher or lower density—the density gradient.[1]

For simplicity, we use the continuous form, but can recover the discrete form by replacing

$$b \to \sum \delta\left(x - X^{(n)}\right)$$

in the formulae. The local density estimate is a weighted function of the distance to others

$$\beta(x) = \iint dx'\, w(x - x')b(x') \tag{4}$$

with the weight function w having compact support and integral one so that a uniform b will give $\beta = b$. The gradient is

$$\nabla \beta = \iint dx'\, \nabla w(x - x')b(x') = \iint dx'\, w(x - x')\nabla' b(x')$$

which indeed gives an estimate of the direction of increase of b.

We will use a weighting function which depends only on distance $r = |x - x'|$ with a range a

$$w(r) = \frac{3}{\pi a^2}\left(1 - r^2/a^2\right)^2$$

and zero for $r > a$. The gradient is

$$\nabla \beta = \iint dx'\, w'(|x - x'|)\frac{x - x'}{|x - x'|}b('x') = \iint dx'\, w_2(|x - x'|)(x' - x)b(x') \tag{5}$$

with

$$w_2(r) = \frac{12}{\pi a^4}(1 - r^2/a^2)$$

---

[1] Social behavior models, especially when observations in the natural habitat are minimal, are necessarily speculative. Copepods clearly exhibit directed swimming in response to pheromones (c.f. [30] and other articles in that volume) as well as hydromechanical and perhaps visual cues. Food distribution might also be a factor.

The preferred swimming velocity $\mathbf{u}_b = -\nabla\phi_b$ will be in the direction of higher neighbor density but at a speed which decreases as the local density increases so that they do not continue to pack rapidly into the center. We use

$$\phi_b = -Ua\frac{\beta}{\beta_0 + \beta}, \quad \mathbf{u}_b = U\frac{a\beta_0\nabla\beta}{(\beta_0 + \beta)^2}$$

with U and β_0 constants. We can choose the units for b such that the half-saturation constant $\beta_0 = 1$; in the rest of the paper, then, b will be the ratio of the density (or number density) to the density at half-saturation.

$$\phi_b = -Ua\frac{\beta}{1 + \beta}, \quad \mathbf{u}_b = U\frac{a\nabla\beta}{(1 + \beta)^2} \tag{6}$$

In an individual-based model, the integrals in equations (4, 5, 6) become sums, and the velocities and positions are advanced using (3). Experiments with this approach indicate that the continuum model is a good representation; we will remark on some differences below.

3.2 Stability of Uniform States

From the equations for the density (in the absence of flow)

$$\frac{\partial}{\partial t}b = \nabla \cdot (b\nabla\phi_b + K_b\nabla b)$$

deviations b' from a uniform state $\overline{b}$ will satisfy

$$\frac{\partial}{\partial t}b' = \nabla \cdot (\overline{b}\nabla\phi'_b + K_b\nabla b')$$

with

$$\phi'_b = -Ua\frac{\beta'}{(1 + \overline{b})^2}, \quad \beta' = \iint d\mathbf{x}'\, w(|\mathbf{x} - \mathbf{x}'|)b'(\mathbf{x}')$$

since β in the uniform state is just $\overline{b}$. For perturbations of the form $b' = A(t)\exp(\iota\mathbf{k} \cdot \mathbf{x})$, we have

$$\phi'_b = -\Phi(|\mathbf{k}|)A(t)\exp(\iota\mathbf{k} \cdot \mathbf{x}), \quad \Phi(|\mathbf{k}|) = \frac{Ua}{(1 + \overline{b})^2}\iint d\mathbf{x}'w(|\mathbf{x}'|)\exp(\iota\mathbf{k} \cdot \mathbf{x})$$
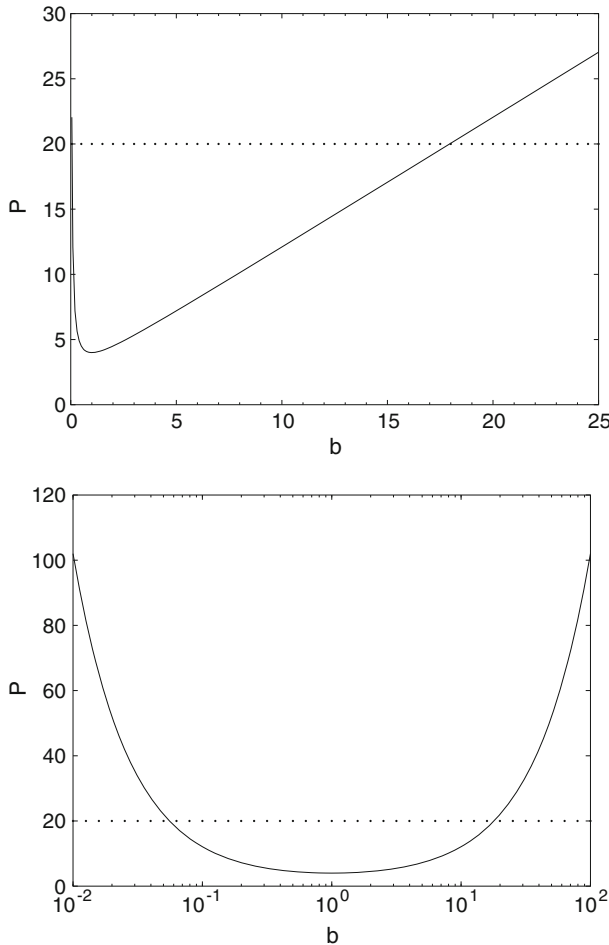
and

$$\frac{\partial}{\partial t}A = |\mathbf{k}|^2(\overline{b}\Phi(|\mathbf{k}|) - K_b)A$$

The transform of the weighting function decays for large $|\mathbf{k}|$, so that diffusion will dominate at short scales; instability can only occur if $\overline{b}\Phi(0) > K_b$. Evaluating the integral at wavenumber 0 gives

$$\Phi(0) = \frac{Ua}{(1 + \overline{b})^2}$$

so that we require

$$Ua\frac{\overline{b}}{(1 + \overline{b})^2} > K_b \quad or \quad P\frac{\overline{b}}{(1 + \overline{b})^2} > 1$$

Fig. 6 Critical values of $\bar{b}$ at different Péclet numbers on a linear or log scale. The uniform state is unstable above the curve. The *dotted line* shows $P = 20$, used in many of the simulations

with $P = Ua/K_b$ the Péclet number for the organism's taxis velocity. This will have a solution for a finite range of $\bar{b}$ as long as $P > 4$ (Fig. 6). The Péclet number here can be thought of as ratio of the directed to random swimming velocity times the ratio of the sensing distance to the mean free path for the random movements; unlike P for the fluid motion, this one is not likely to be very large.

FINITE AMPLITUDE:

The growth of perturbations and the formation of patches is illustrated in Fig. 7; the patches equilibrate fairly quickly, and then mergers take place over a much longer time. All simulations are in a doubly-periodic domain. The merger process in the continuum model can be viewed as follows: a patch has a long, but exponentially weak, tail which produces a small attractive velocity on neighboring patches. Merger also occurs with the individual-based model, but it is more rapid because the stochastic motion leads to wandering of the patches.
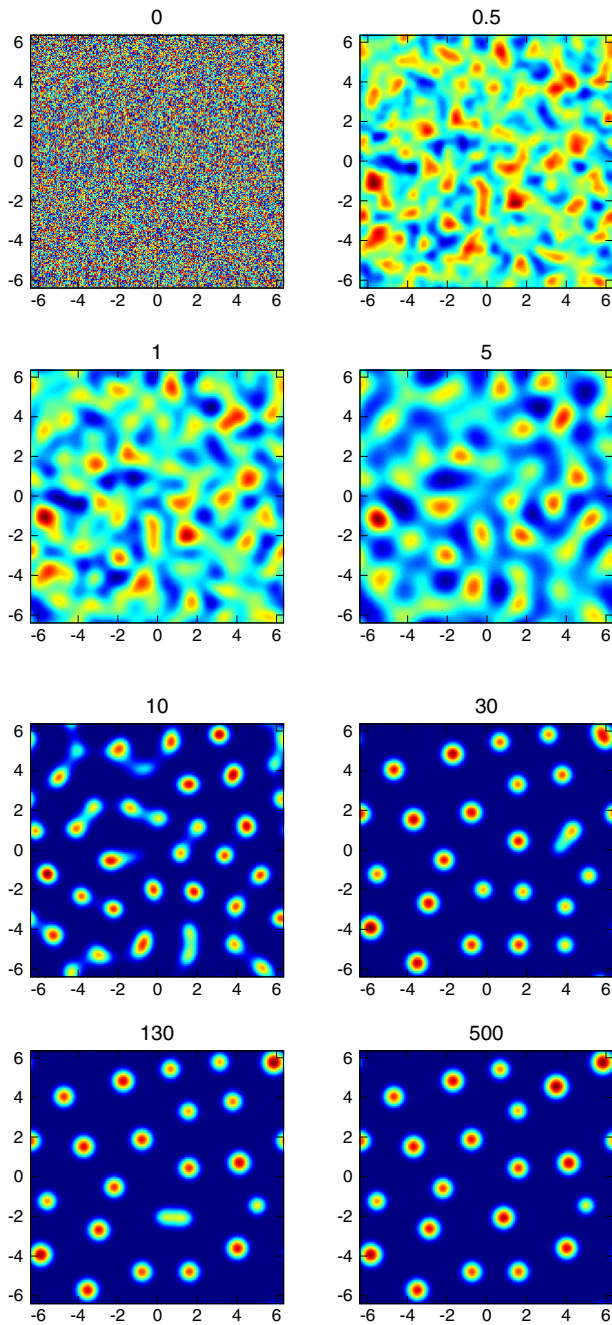
Fig. 7 Densities $b(x, y)$ with Péclet number $Ua/K_b = 20$. Mergers can be seen in progress at $t = 10, 30, 130$. Note also the decrease in the number of patches and the increase in size from $t = 10$ to $t = 500$
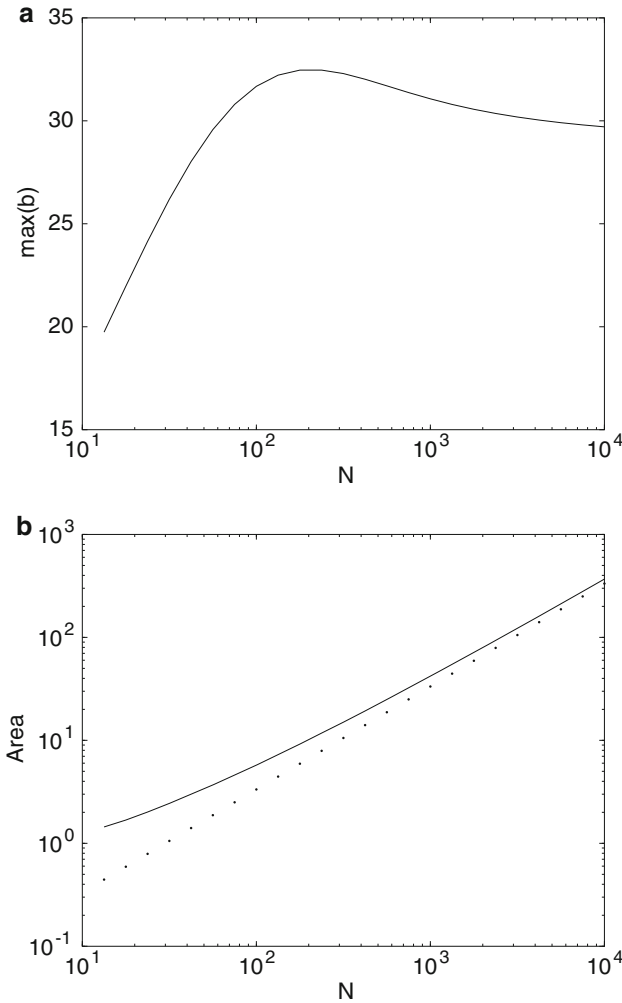
Fig. 8 Steady states versus $N = \iint b$. **a** Maximum density. **b** Patch area with *dotted line* showing a linear relationship $N/30$. The Péclet number is 20

PATCH SIZES: In the previous experiment, as mergers take place, the maximum value of b does not increase by much; instead the area grows. For social behavior and constant K_b, we still have that steady states (first without flow) satisfy

$$b = b_0 \exp(-\phi_b/K_b) = b_0 \exp\left(P\frac{\beta}{1+\beta}\right)$$

We can find steady states by iterating: from a guess of b with $N = \iint b$, we calculate β and then compute $\hat{b} = \exp(P\beta/[1+\beta])$. The factor b_0 is then chosen as $N/\iint \hat{b}$. This gives a new estimate of b, and we can repeat until it converges. A finite domain size is required, so that N can be finite even with $b_\infty > 0$. The domain size does not seem to have much effect until the average b approaches the stability boundary. For example, $N = 3$ converges in a

Fig. 9 Densities $b(x, y)$ with
Péclet number $Ua/K_b = 20$ at
$t = 250$. The *upper panel* shows
the case without shear; the *lower*
has $u = 0.1\sin(2\pi y/W)$ with
the domain width $W = 12.8$ (the
range of the weighting function is
one)

$U_s = 0$

$U_s = 0.1$
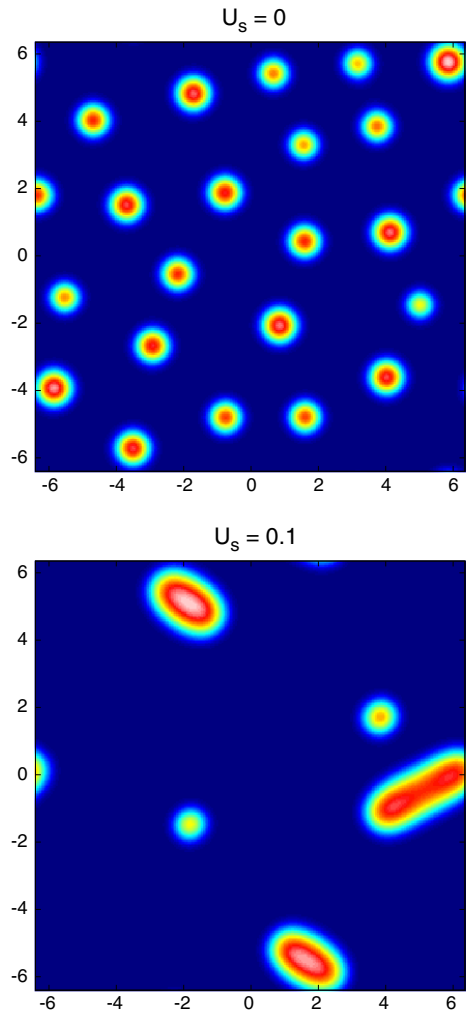
6.4×6.4 area but not in 12.8×12.8; on the other hand $N = 100$ looks identical over a two
orders of magnitude increase in the area.

We have verified these by time-marching, starting with all the organisms within a circle
of small enough radius such that the density is above the high cutoff of the unstable range.
The patch remains circular, and the amplitude reaches the value in Fig. 8. When we add
a random field over the domain, the big patch still forms up into a steady profile with the
same amplitude, while the outer region is filled with small patches like those in Fig. 7. These
experiments show that this social dynamics is consistent with having large, stable patches.

SHEAR: As a simple test of whether "stickiness" and shear resistance are indeed displayed
by this model, we simply add a steady shear flow $u = U_s \sin(k_0 y)$ to the biological velocity $\mathbf{u}_b$.
We compare the states starting with the same random initial conditions (uniform distribution
on 0 to 1) with $U_s = 0.1$ compared to the scale $U = 1$ for ϕ_b. The shear has indeed led
to coagulation and many fewer and larger patches. As Fig. 9 suggests, however, the patches
can break up again; watching the development shows that the patches centered at slightly

different y values move towards each other, merge into an elliptical structure but then this rotates in the shear, the ends are drawn apart, they separate, and then form back into smaller, more circular patches as they move away from each other.

4 Combined Effects in More Complex Flows

Unlike the purely physical problems where ϕ can become large and positive so that $\exp(-\phi/K)$ can decay towards zero, the social model has ϕ_b always negative so that in a steady state $b \geq b_0 > 0$. Indeed, if b becomes constant, b_∞, in the far field

$$b_\infty = b_0 \exp\left(P \frac{b_\infty}{1 + b_\infty}\right)$$

If b_∞ is very small, this yields $b_0 = b_\infty/(1 + P b_\infty)$ allowing us to relate the unknown coefficient b_0 to the far field value or vice-versa. An important conclusion is that the patch does not cut off with zero concentration outside. Indeed, even though the sensing radius is finite, u_b can be shown to decay exponentially away from the patch without cutting off. Thus, different patches indeed can interact by their far fields which have gradients that can attract other patches, albeit exponentially small ones. The far field also affects the response to strain.

A pure strain field $\phi = \frac{1}{2}S(y^2 - x^2)$, in the passive case, led to growth as an initial disturbance compressed in along the y axis and then decay as it leaked out along the x axis. When we add this to the biological ϕ_b and try to iterate to a steady state, we find that the solution for small enough S appears to converge, but then the difference between successive iterations begins to grow again, and the patch separates into two blobs heading in opposite directions in x (or breaks symmetry into one blob moving either right or left).

In essence, the social attraction is not able to entirely prevent the losses along the axis of extension. The exponential tails will extend into a region where the outward flow from the physics overwhelms the weak, inward, far-field flows from ϕ_b. The leakage is slow, since b is exponentially small in the wings of the patch; therefore, temporal changes in the flow field may again play a significant role.
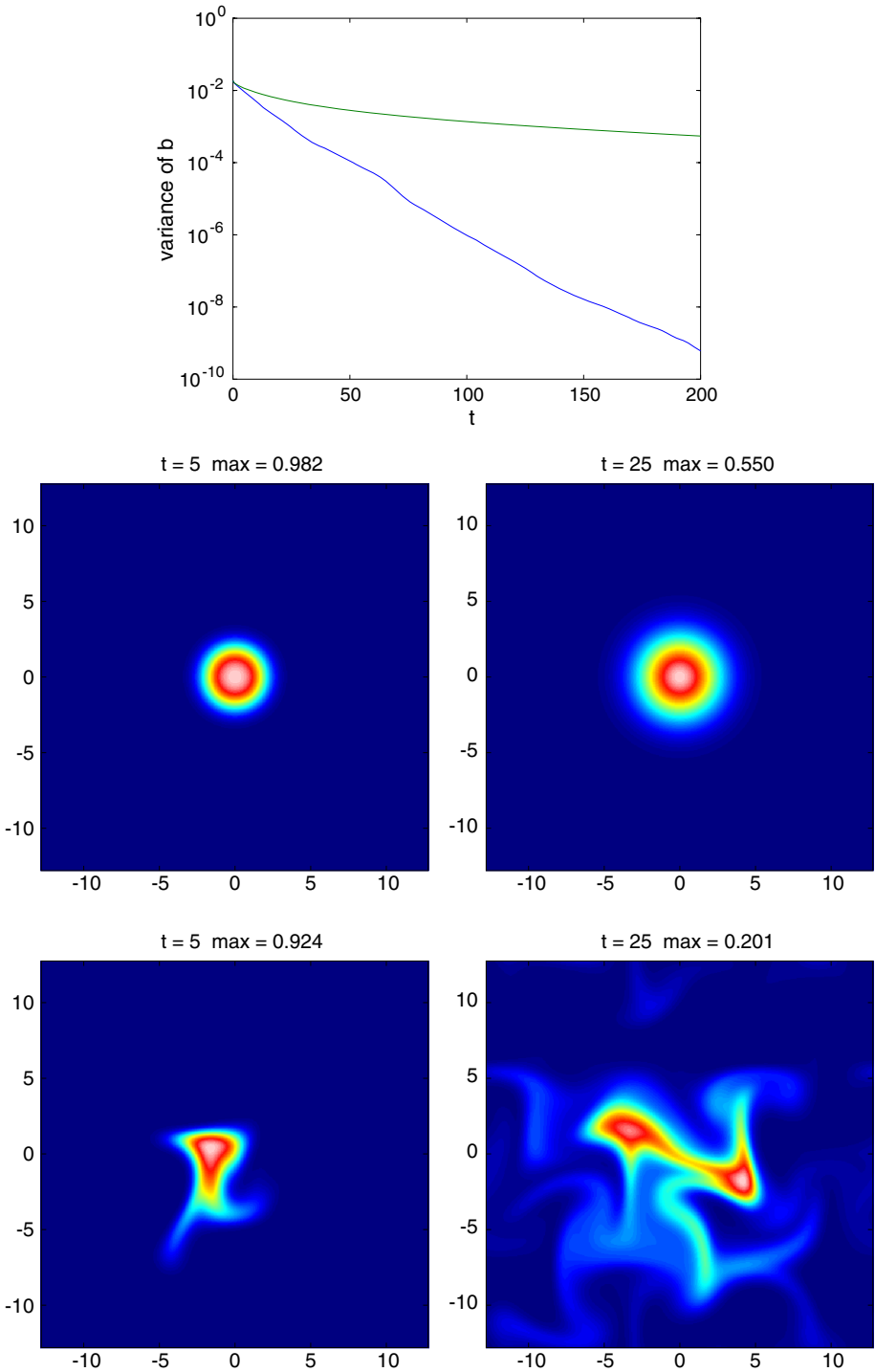
4.1 Stirring

Ocean flows are variable in both space and time, and, as we have suggested, the combination may inhibit buildup by purely physical processes. To explore the implications of more turbulent flows, we have used a simple stirring process defined by a streamfunction

$$\psi = \frac{U_s}{k\sqrt{7}}\left[\cos\left(kx + \frac{\theta_{x1}}{3}\right)\cos\left(ky + \frac{\theta_{y1}}{3}\right)\right.$$

$$\left. + \cos(2kx + \theta_{x2})\cos(3ky + \theta_{y2}) + \cos(3kx + \theta_{x3})\cos(2ky + \theta_{y3})\right] \quad (7)$$

where $k = 2\pi/W$ and the variables θ_{xj} and θ_{yj} undergo independent random walks with $\delta\theta = 0.02$ for a time step of 2^{-9}. The normalization makes U_s the r.m.s. velocity for the eddies.

Figure 10 compares the decay of the variance in b for an initial patch with amplitude $b = 1$ for $\sqrt{x^2 + y^2} < 3$ and zero outside under pure diffusion and under the stirring. The shears in the velocity quickly stretch the patch into filaments which then diffuse rapidly because of their small scales; as evident in Fig. 10.

Fig. 10 Decay of the variance for the stirring case (*lower*) and the purely diffusive case (*upper*). Plots at $t = 5$ and $t = 25$ of the distributions of b normalized by the maximum values listed in the titles

When we add social behavior, we find the individual patches will again encounter each other and aggregate, as in the steady shear case, though they can be broken back up by the shears.

4.2 Stirring and Convergence

To model the joint effects of stirring and convergence, we want to use a physically motivated relationship between ψ and ϕ. For ocean eddies and jets, Coriolis forces are usually dominant, and the vertical velocities are weak. The vertical vorticity $\zeta = \frac{\partial v}{\partial x} - \frac{\partial u}{\partial y} = \nabla^2 \psi$ then approximately satisfies

$$\left(\frac{\partial}{\partial t} + \mathbf{u} \cdot \nabla \right) \ln(\zeta + f) = s$$

Combining this with the non-diffusive form of the b equation implies that $b/(\zeta + f)$ is conserved following the horizontal flow. Usually $|\zeta|$ is smaller than $\frac{1}{2} f$ so that even a swing from a strong anticyclone to a cyclone would involve a stretching that would only amplify b by a factor order 3. This argument, though over-simplified, indicates the importance of considering the dynamics of the flow, not just the kinematics.

When the streamlines and vorticity field are nearly aligned, we can use

$$\frac{\partial}{\partial t} \zeta = \frac{\partial}{\partial t} \nabla^2 \psi \simeq f \nabla^2 \phi$$

with bottom Ekman friction [21], $\frac{\partial}{\partial t} \zeta = -\sigma \zeta$ so that $\phi = -(\sigma/f)\psi$. For organisms living in the bottom boundary layer, the proportionality constant is $+\frac{1}{2}$: in essence, the bottom stress, which opposes the flow above the bottom boundary layer, is balanced by the Coriolis force acting on the inward or outward flow. The convergence (under a cyclone) produces upwelling out of the boundary layer; in the fluid above, there is a corresponding, but weaker by the ratio of the depth to the boundary layer thickness, divergent (cyclone) or convergent (anticyclone) flow with ϕ proportional to $-\psi$. Note that irrotational flows like $\psi = -U_0 y$ will not have upwelling or an associated ϕ.

We show two examples combining the various elements we have discussed: physical convergence, social behavior, and stirring. The first case has a localized, steady anticyclonic circulation and a uniform flow added to the time-dependent stirring (Eq. 7).

$$\psi_{tot} = \psi_{stir} + U_0 L_0 \exp\left(-\frac{1}{2} |\mathbf{x}|^2 / L^2 \right) - 0.2 U_0 y$$

We set the potential to $-\alpha \psi$ (except for the uniform flow term). In Fig. 11, we show an example where the proposed mechanism seems to work especially well. The social behavior creates small, but high density patches, the stirring brings these into the region with consistent convergence where they merge to form a large patch. The patch occasionally loses bits at the edge but 80–90 percent of the organisms remain in it.

However, even this system has a large number of parameters, and the behavior is indeed sensitive to their values. We have chosen the time and length scales based on swimming velocity U and the perception radius a. The remaining parameters in this experiment are the biological diffusion $K = 0.05$ ($P = 20$), the strength of the steady anticyclone $U_0 = 0.15$,
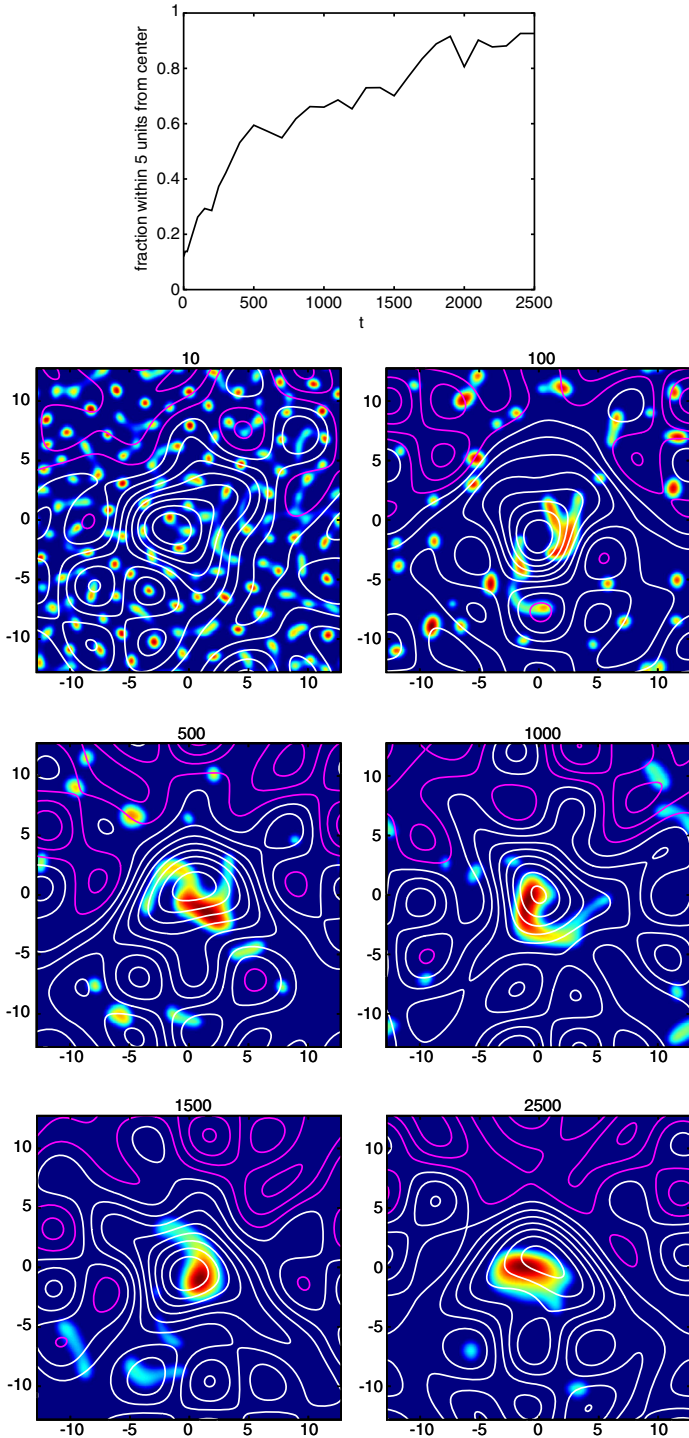
Fig. 11 Fraction of organisms in $r < 5$ and snapshots at various times. The *contour lines* are the streamfunction with negative values in magenta (Color figure online)
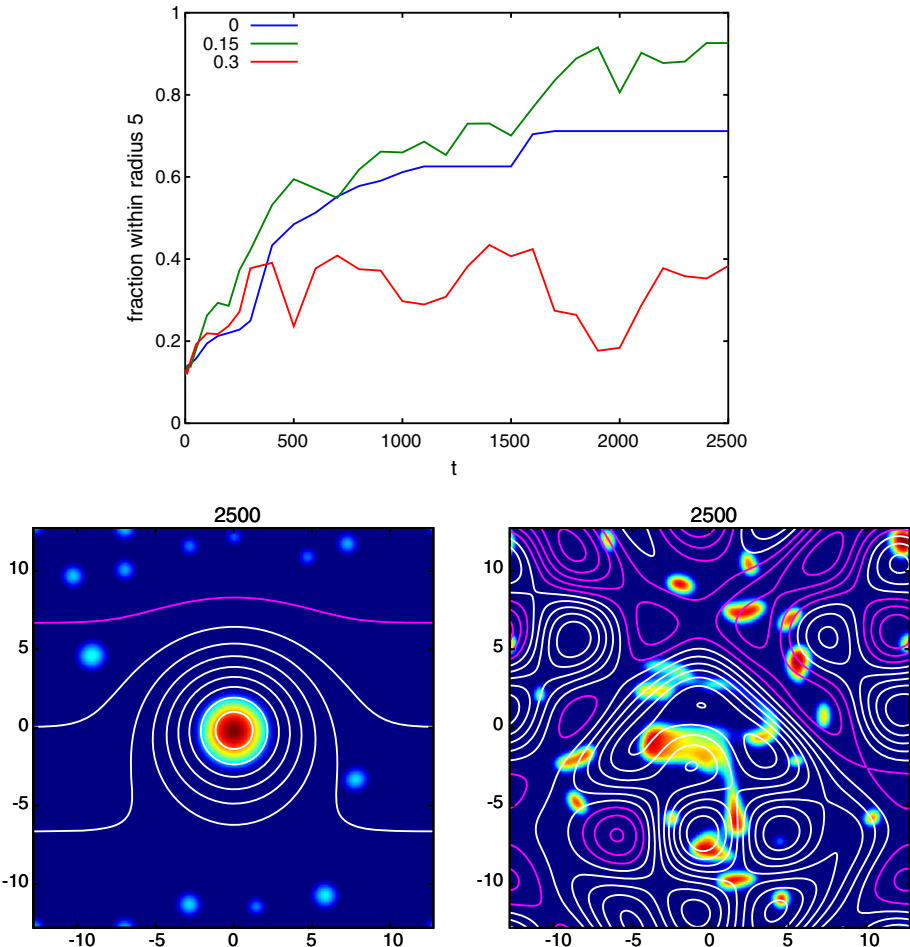
Fig. 12 Fraction in the central region for various stirring flow strengths. *Lower plots* show the state at $t =$ 2,500 for $U_s = 0$ and $U_s = 0.3$; compare to the last plot in Fig. 11

and of the stirring $U_s = 0.15$. The ratio of $\alpha = \phi/(-\psi)$ is 0.1, and the various length scales are $L = \sqrt{10}$ and $1/k = 4.1$.

If the stirring is increased relative to the stationary flow, the large patch experiences more strain and cannot stay together. Blobs are lost to outside of the convergence region and others are re-entrained (Fig. 12).

As a second example we consider a front with

$$v = U_0 \operatorname{sech}^2(y/3), \qquad \phi_p = -0.3\, U_0 \operatorname{sech}^2(y/3)$$

but with no convergence associated with the stirring part of flow (Eq. 7). The results are very similar (Fig. 13): without social behavior, we have a broad area of convergence with an amplification factor of about 9; with grouping, the amplitude is about 34, with a finer filament meandering around the center of the front and occasionally breaking up.
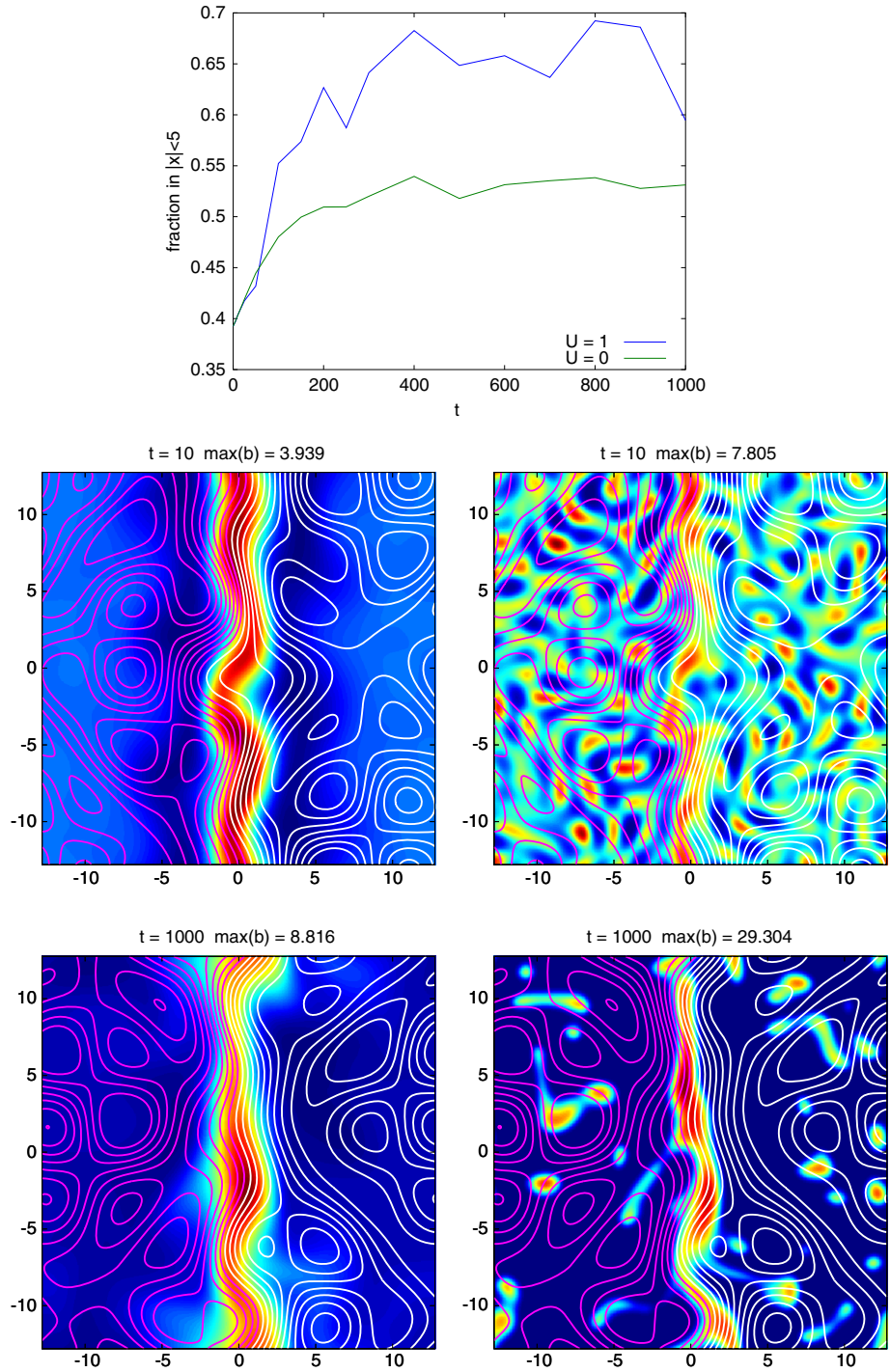
Fig. 13 Fraction of population in jet region with and without social behavior. The *lower panels* show *b* at *t* = 10, 1000 with the *U* = 0 case on the *left* and *U* = 1 on the *right*

5 Discussion

The experiments presented here and in [29] indicate that indeed the physics by itself will not compress material by several orders of magnitude—the turbulence we've invoked to bring tracer from a large area through the convergent region will, for passive tracers, also be effective at stirring it back out. If we think of turbulence as enhanced diffusivity, the $\exp(-\phi/K)$ form suggests it would lead to low densities, consistent with the way stirring acts in our simulations. Attraction of individuals (and on the larger scale, of groups) can provide a means for resisting this spreading. Our model for the social behavior has the property that the maximum concentration is not sensitive to the size of the patch; even though a large aggregation may be torn apart by shears, the pieces still have high density and can remain in the same geographic area. Indeed, the kilometer scale patches may, in fact, be heterogeneous with local very high density aggregations within an overall elevated level.

The theory and simulations support the idea that both physics and social behavior play a role in the observed large aggregations of copepods. The small patches from social behavior can indeed be brought in contact by eddies and merge to form larger aggregations. Localized convergence, with inward flow which vanishes far from the center, can accumulate the patches in an area, with turbulence bring ones from outside of the convergent region close enough that they can then be entrained into the large aggregation. On the other hand, the stirring does disrupt the large patches, breaking them apart if they hit a temporary stagnation point or peeling off small blobs. These calculations suggest we might expect to find regions with larger patches and more of them, but that this state may not be long-lived and may still remain heterogeneous, especially around the edges.

Although our model has a range of scales, it cannot go from the perhaps centimeter scales of the sensing distance to the kilometer scales which patches seem to cover. We suspect that some form of renormalization may succeed here: perhaps, the figures can be reinterpreted as the density of smaller groups rather than of individuals. Although the coagulation of groups is quantitatively different from group formation, it clearly happens (though more slowly as they get larger). In the individual-based model, the coagulation is more rapid, but groups can spontaneously split; however, this seems to be less of an issue as they get larger. At each stage—going from individuals, to groups, to groups-of-groups, up to kilometer scale patches—the process is going to depend on the strength of the turbulent flows at that scale and on the magnitude of the frontal (or other) convergence. And the postulate that the total number over the area which could feed into a convergent zone is not increasing implies that we must ascribe the high densities to aggregations which are narrow compared to the convergence zone. In the frontal experiment, that indeed occurred and was driven by the social behavior.

Given the importance of copepod aggregations for whale feeding, we would certainly like to understand and predict them better; data on both spatial and temporal structure of the density and of the flow fields would be tremendously helpful. The theoretical/ numerical approach also has a number of issues which are as yet unresolved: the actual behavior which can lead to patchiness, the range of scales involved, and the structure of the stretching field (and suitable de-tiding).

Appendix 1: Vertical Swimming

For organisms swimming vertically at a speed $w_s(z, t)$ with random variations producing a "diffusion" $K_s(z, t)$ (presuming both have significant variation only in z), the density satisfies

$$\frac{\partial}{\partial t}b + \nabla \cdot (\mathbf{u}b - K\nabla b) + \frac{\partial}{\partial z}\left([w + w_s]b - [K_s + K_v]\frac{\partial}{\partial z}b\right) = 0$$

(with $\mathbf{u}$ and ∇ being horizontal and w, K_v being the physical vertical motion and mixing, respectively). We assume that the vertical swimming is strong and convergent at some preferred depth (including the surface or bottom). The lowest order dynamics (neglecting time-variation of the swimming) is

$$\frac{\partial}{\partial z}\left(w_s b - K_s\frac{\partial}{\partial z}b\right) \simeq 0$$

Then b will take the form $\tilde{b}(\mathbf{x}, t)F(z)$ with

$$\frac{\partial}{\partial z}\ln F = w_s/K_s$$

(like Eq. 2 but in the vertical). If the swimming propels the organisms up or down towards a particular depth and is rapid, the vertical scale of F, K_v/w_s, will be small, and F will be sharply peaked around the preferred depth (by analogy to Fig. 1). Using the $\tilde{b}F$ solution to iterate on the original equation gives

$$\frac{\partial}{\partial z}\left(w_s b - K_s\frac{\partial}{\partial z}b\right) = -F(z)\left[\frac{\partial}{\partial t}\tilde{b} + \nabla \cdot (\mathbf{u}\tilde{b} - K\nabla\tilde{b})\right] - \tilde{b}\frac{\partial}{\partial z}\left(wF - K_s\frac{\partial}{\partial z}F\right)$$

Since we are interested in the net biomass, we shall normalize F by taking $\int dz\, F = 1$ and integrate the equation above. There is no flux through the boundaries and w vanishes as well. We arrive at the equation for $\frac{\partial}{\partial t}\tilde{b}$ in the text with divergent horizontal flows $\tilde{\mathbf{u}}$ and associated stretching.[2]

Appendix 2: Circular and Non-Symmetric Geometries

When the streamfunction, potential, and boundary conditions are all independent of θ, we again have

$$b = b_0 \exp(-\phi/K)$$

We can solve the same problems, just replacing x by r and limiting the domain to be $r \geq 0$. We argue in Sect. 4.2 that $\phi \sim \psi$ so that an isolated eddy can be expected to have localized radial velocities as well. In this case, the far field can have a finite background value, and the steady state solution has a central amplitude order $\exp(P)$ larger. But, as Appendix 3 shows, this buildup happens in two stages: first, the patch gets denser by drawing in the organisms out to where the velocity peaks and depleting the annulus where convergence occurs. Then the peak value changes more slowly, on a time scale L^2/K, because of diffusion into the depleted area and then into the center until the convergence and diffusion balance (Table 2).

If the symmetry is broken, the flux F_0 will no longer be zero. The steady solution now has

$$ub - K\frac{\partial}{\partial x}b = F_0$$

so that

$$b = b_s - b_s\int_{x_0}^{x}\frac{F_0}{Kb_s}$$

---

[2] When the swimming is time-dependent but the time for forming a layer remains short, we would just end up integrating $F(z, t)\mathbf{u}$, introducing additional time-dependence in $\tilde{u}$.

Table 2 Radial flow

Description	Flow	Density
1. Pure strain	$u = -Ur/L$	$b = b_0 \exp\left(-\frac{1}{2} P \, (r/L)^2\right)$
2. Localized convergence	$u = -U_0 \tanh(r/L)$	$b = b_0 \mathrm{sech}^P (r/L)$
3. Localized u	$u = -U(r/L) \exp\left(-\frac{1}{2}(r/L)^2\right)$	$b = b_0 \exp\left(Pe^{-\frac{1}{2}(r/L)^2}\right)$

where b_s is the homogeneous solution, with amplitude chosen to match the condition at x_0. The flux F_0 is chosen to match the right boundary condition.

The solution (Eqs. 2a, 2b) will also apply to other steady flow cases. When contours of ϕ, K, and ψ are parallel, the form

$$\nabla \ln(b) = -\frac{1}{K(\phi)} \nabla \phi$$

gives a flux

$$\mathbf{F} = u_\psi b - b\nabla\phi - K\nabla b = u_\psi b$$

The divergence of the flux is

$$\nabla \cdot \mathbf{F} = \nabla \cdot (\mathbf{u}_\psi b) = \mathbf{u}_\psi \cdot \nabla b = -\frac{b}{K} \mathbf{u}_\psi \cdot \nabla \phi$$

which vanishes under the stated assumptions.

In the circular geometry, the rotational flux will have a contribution if the boundary or initial conditions vary with angle. For example, if b is not constant on some closed ϕ contour, the solution above cannot hold. The strong flow case seems most relevant: when the rotational flow is large compared to the convergent flow, the density will homogenize along streamlines by shear dispersion and then slowly diffuse and converge across them. This argument is based on the Prandtl-Batchelor theorem [1]. The lowest order solution to

$$\frac{\partial}{\partial t} b + \mathbf{u}_\psi \nabla \mathbf{b} = \nabla \cdot (b\nabla\phi + K\nabla b)$$

is just

$$(\hat{\mathbf{z}} \times \nabla \psi) \cdot \nabla b = 0$$

which implies $b = b(\psi, t)$. Integrating the equation over the area enclosed by two streamlines gives

$$\frac{\partial}{\partial t} \iint b = \oint_{\psi_0 + d\psi} \hat{\mathbf{n}} \cdot (b\nabla\phi + K\nabla b) - \oint_{\psi_0} \hat{\mathbf{n}} \cdot (b\nabla\phi + K\nabla b)$$

If we use the approximation that $b = b(\psi, t)$ and take $d\psi$ to be small, this becomes

$$\frac{\partial}{\partial t} b \oint_{\psi_0} |\nabla\psi|^{-1} = \frac{\partial}{\partial \psi} \left\{ b \oint_{\psi_0} \frac{1}{|\nabla\psi|} \nabla\psi \cdot \nabla\phi + \left[\oint_\psi K|\nabla\psi| \right] \frac{\partial b}{\partial \psi} \right\}$$

(c.f., [23]). This 1D advection-diffusion equation has much the same character as the cases discussed previously; the exception would be if there is a stagnation point in $\mathbf{u}_\psi$ which corresponds to a singularity in the time for transiting the contour – which is the coefficient of
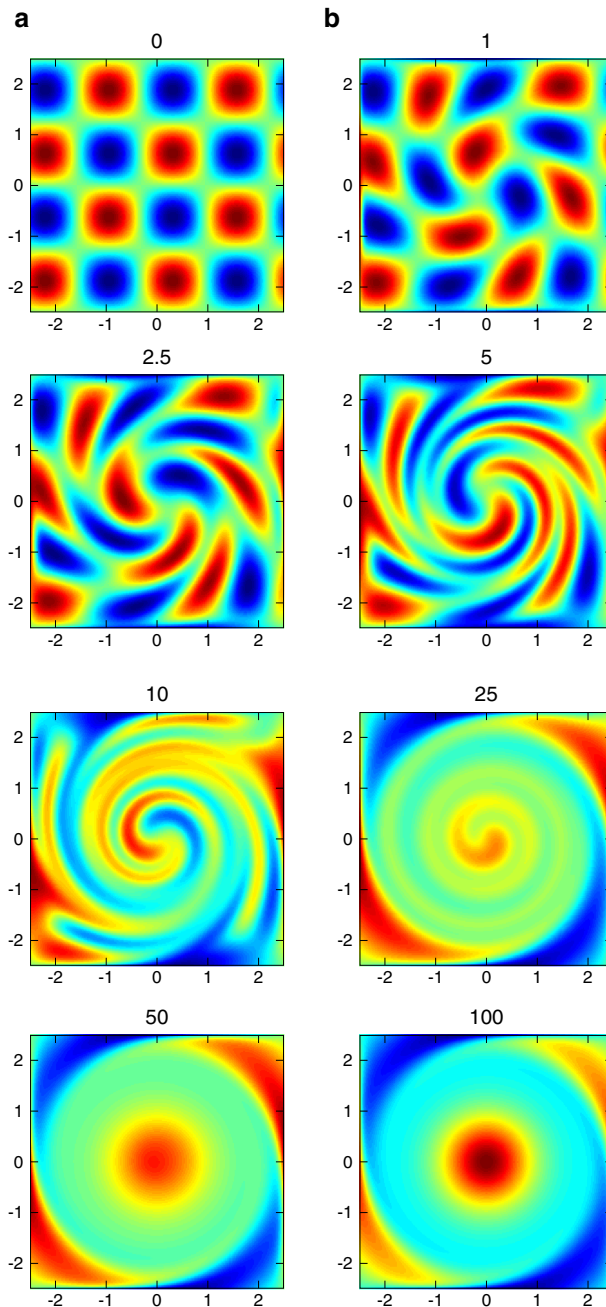
Fig. 14 a The homogenization process for Péclet number 10 and $\psi = 1.67\phi$. $t = 0, 1, 2, 5$. **b** Later times. $t = 10, 25, 50, 100$. The boundary conditions are maintained at the value shown in the first frame; this asymmetry remains at later times, but only in regions near the boundary

$\frac{\partial}{\partial t}b$. The assumption of rapid movement along streamlines compared to the diffusion or cross streamline flow clearly breaks down there, but, as [8] argued, it does not make a significant difference. We still expect to find b will tend towards

$$b = b_0 \exp\left(-\int^\psi d\psi \, [U(\psi)/\mathcal{K}(\psi)]\right)$$

but with the divergent flow and effective diffusivity suitably weighted by the along-streamline velocity

$$U = -\oint_{\psi_0} \frac{1}{|\nabla\psi|}\nabla\psi \cdot \nabla\phi, \quad \mathcal{K} = \oint_\psi K|\nabla\psi|$$

Figure 14 shows this process with a Gaussian ψ, starting from a checkerboard pattern, which then becomes spirals and converges into the middle. The maximum amplitude at the last time shown is still only 5.6 times the boundary value; it will climb to order e^{10}.

Appendix 3: Time-Dependent Problems

Even in the case with symmetric boundary conditions, the localized flow problem has several different time scales (Fig. 15). Initially, the patch gets denser by drawing from the surrounding annulus where the velocity peaks and it compresses into the center. This occurs with a time scale of order L^2/ϕ_0; then the peak value changes more slowly because of diffusion in or out of the boundary on a time scale L^2/K. The distribution finally stabilizes at

$$b = b_\infty \exp\left(-\int_r^\infty dr \, \frac{u}{K}\right)$$

as shown in Fig. 15.

The solutions with non-zero inflow in the far field can only settle to a steady solution if the population initially extend over a finite area: if b is non-zero as x or $r \to \pm\infty$, the flows will continue to import organisms into the system. In the pure strain case, beginning with uniform b is not very physical: it leads to simple exponential growth with time everywhere $b = b(0)\exp(Ut/L)$. The localized front case is more interesting because the far-field population remains constant. For the special case when the Péclet number is equal to 2, $U_0 = 0$, and the population is uniform at $t = 0$, there is a simple analytic solution to the time-dependent problem:

$$b = b(0) + b(0)\frac{Ut}{L}\text{sech}^2(x/L)$$

The second term is just the steady-state solution but with amplitude growing linearly in time as new organisms are brought in from further and further away. To reach amplitudes 100 times the background $b(0)$, the flow has to be sustained and far-reaching enought to bring organisms from a distance 100 times the front width. Indeed, if we ignore diffusion entirely, the solution is just

$$b = b(0)\frac{\cosh(x/L)e^{tU/L}}{\sqrt{\sinh^2(x/L)e^{2tU/L} + 1}}$$

At the origin, this grows exponentially, but a short distance away, the concentration asymptotes to $|\coth(x/L)|$ which is only 1.3 for $x = L$ or 4 for $x = \frac{1}{4}L$. from the expression for the ratio

$$R = b(x, t)/b(x, \infty) = \frac{\sinh(x/L)e^{tU/L}}{\sqrt{\sinh^2(x/L)e^{2tU/L} + 1}}$$
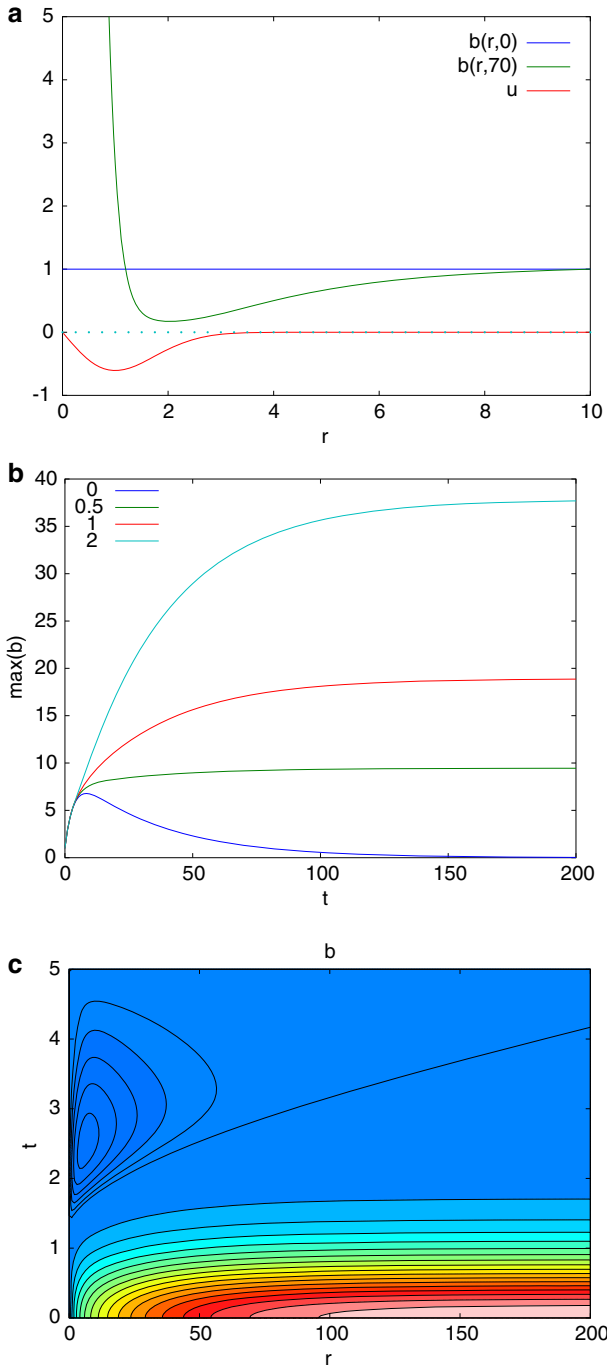
Fig. 15 **a** The initial condition and the density at $t = L/U$ as functions of r/L, showing the depletion of the annular region. ($P = 10$ for this plot; $b(0, 70) = 97.3$. **b** The growth of the maximum for various boundary values. Time is non-dimensionalized by L/U and $P = 3$. The initial value of b is one. **c** The evolution of b versus tU/L and r/L. Contours are at $b = 0.75, 0.8, \ldots, 0.95, 1, 2, \ldots, 18$

it is clear that the time to approach large amplitudes (meaning small values of x) behaves like $-L/U \ln(\sinh[x/L]) \sim (L/U) \ln R$ and increases significantly. In the presence of diffusion, we see growth at x (away from zero) by advection like that above until ub is nearly constant and then a slower phase where diffusion is spreading the central peak.

Frontal models of accumulation often have localized convergence but velocities extending far from the front (e.g., [10] have a $-\tanh(x)$ flow); these models argue that the accumulation will be modest if the front has localized velocities or lasts for times which are not tremendously long compared to $L/|\nabla\phi|$.

Appendix 4: Advective Losses

To understand advective losses, consider the movement relative to the plume: the organisms approach the front, but are left in the surface as the denser water goes under the plume (really
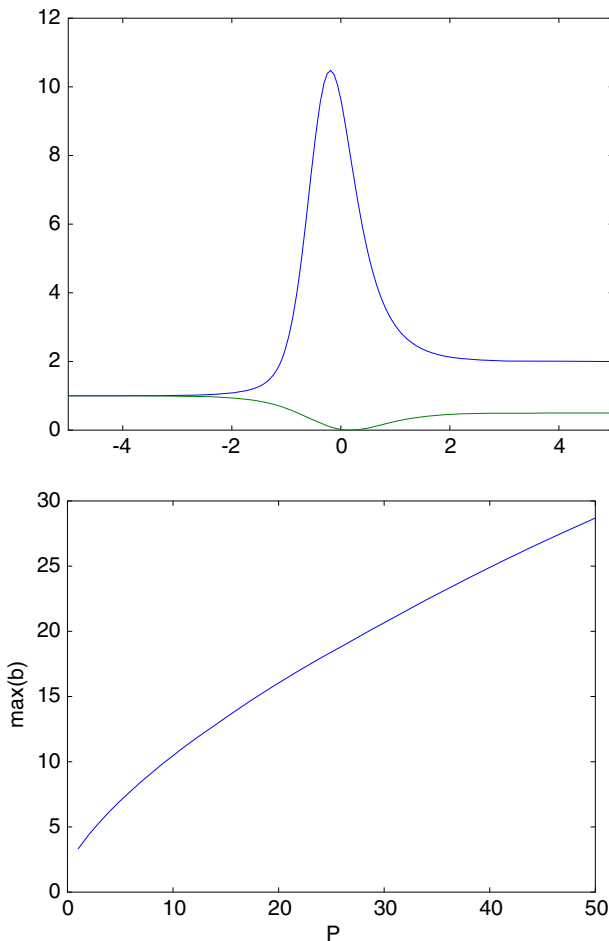
Fig. 16 Density $b(x)$ for $a = 0.25$ and the associated velocity. The *lower figure* shows the peak value as a function of P
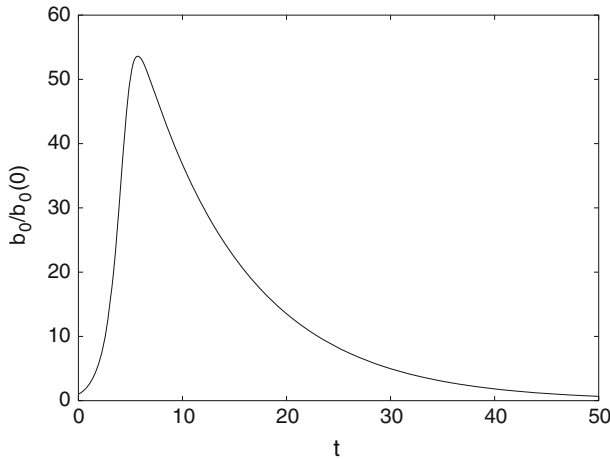
Fig. 17 Changes in concentration for a pure strain field with $A = 1$, $B = -0.1$, $K = 0.01$ with initial values $\alpha = \beta = 0.01$

the plume riding over relatively still water). But they can diffuse through the front to be picked up by the plume-relative flow inside or be swept along the front. In a 1D model, we can think of this as a localized convergence but with different velocities on each side. For $u = U_0 - U \tanh(x/L)$ with $U_0 > U$, the concentration transitions smoothly and monotonically from its upstream value $b(-\infty)$ to the downstream value $b(\infty) = b(-\infty)(U_0+U)/(U_0-U)$ which gives the same flux $ub - K \frac{\partial}{\partial x} b = u(-\infty)b(-\infty)$. The amplification is independent of P. If we use a slightly more complex velocity which drops to zero at the front, but picks up on the other side

$$u/U = 1 - a - a \tanh(x) - \frac{1 + \sqrt{1 - 2a} - a}{2} \operatorname{sech}^2(x)$$

the concentration far downstream is still enhanced by $u(-\infty)/u(\infty) = 1/(1 - 2a)$, but the temporary blockage caused by slow diffusion across the front gives a local peak; however the amplitude increases only roughly linearly in P rather than exponentially (Fig. 16).

In two dimensions, advective losses can be even more significant. Consider a strain field like that which may occur near the intersection of the nose with the wall. Relative to the moving plume, the velocity would look like
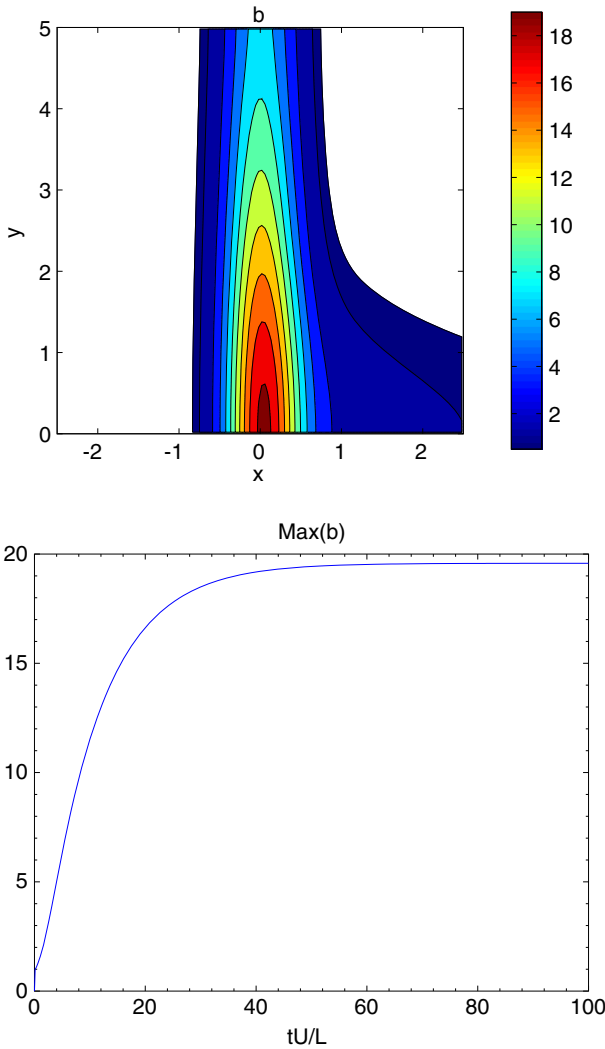
$$\mathbf{u} = (-Ax, -By)$$

where either coefficient could be negative or zero. The potential is

$$\phi = \frac{1}{2}Ax^2 + \frac{1}{2}By^2$$

and we will only reach an appropriate steady state $[\exp(-\phi/K)]$ if both A and B are positive. We shall look for Gaussian solutions

$$b = b_0(t) \exp\left(-\frac{1}{2}\alpha(t)x^2 - \frac{1}{2}\beta(t)y^2\right)$$

Fig. 18 Final density $b(x, y)$ for $B = -0.1$, $P = 10$ with $b(2.5, y, t) = \exp(-\frac{1}{2}y^2)$. The *lower figure* shows the peak value versus time

This leads to three equations

$$\frac{\partial}{\partial t}\alpha = 2\alpha(A - K\alpha)$$

$$\frac{\partial}{\partial t}\beta = 2\beta(B - K\beta)$$

$$\frac{\partial}{\partial t}b_0 = [A - \alpha K + B - \beta K]b_0$$

The equations for α and β are the logistic equations; if B is positive, β will initially grow exponentially and then asymptote to A/K. But if $B < 0$, then β decays to zero and the

width in that direction becomes infinite. Combining the three equations shows that $b_0/\sqrt{\alpha\beta}$ is constant. Thus, if both scales limit to finite values, b_0 will also. If either A or B is negative, the patch cannot resist the divergence in that direction and the amplitude will decay to zero. However, when that coefficient is small, we can have substantial amplification and then a slow decay (Fig. 17).

Even if the "upstream" population is maintained in a band near the coast (i.e., the front is moving into a region with some background concentration), the peak concentration levels off in much the same way as in the 1D problem (Fig. 18). This example shows that advective losses can be an important limiter on the density enhancement associated with convergence.

References

1. Batchelor, G.K.: Steady laminar flow with closed streamlines at large Reynolds numbers. J. Fluid Mech. **1**, 177–190 (1956)
2. Baumgartner, M.F., Cole, T.V., Clapham, P.J., Mate, B.R.: North Atlantic right whale habitat in the lower Bay of Fundy and on the SW Scotian Shelf during 1999–2001. Mar. Ecol. Prog. Ser. **264**, 137–154 (2003)
3. Baumgartner, M.F., Mate, B.R.: Summertime foraging ecology of North Atlantic right whales. Mar. Ecol. Prog. Ser. **264**, 123–135 (2003)
4. Beardsley, R., Epstein, A., Chen, C., Wishner, K., Macaulay, M., Kenney, R.: Spatial variability in zooplankton abundance near feeding right whales in the Great South Channel. Deep Sea Res. Part II **43**, 1601–1625 (1996). doi:10.1016/S0967-0645(96)00050-1
5. Birch, D.A., Young, W.R., Franks, P.J.S.: Thin layers of plankton: formation by shear and death by diffusion. Deep-Sea Res. I **55**, 277–295 (2008)
6. Birch, D.A., Young, W.R., Franks, P.J.S.: Plankton layer profiles as determined by shearing, sinking, and swimming. Limnol. Oceanogr. **54**, 397–399 (2009)
7. Chen, C., Liu, H., Beardsley, R.: An unstructured grid, finite-volume, three-dimensional, primitive equations ocean model: application to coastal ocean and estuaries. J. Atmos. Ocean. Techn. **20**, 159–186 (2003)
8. Dewar, W.K., Flierl, G.R.: Particle trajectories and simple models of tracer transport in coherent vortices. Dyn. Atmos. Oceans **9**, 215–252 (1985)
9. Epstein, A.W.: Physical processes and zooplankton distribution in the great south channel: Observational and numerical studies. Ph.D. Thesis, MIT/WHOI Joint Program in Physical Oceanography (1995)
10. Epstein, A.W., Beardsley, R.C.: Flow-induced aggregation of plankton at a front: a 2-d Eulerian model study. Deep Sea Res. Part II **48**, 395–418 (2001)
11. Flierl, G., Grünbaum, D., Levin, S., Olson, D.: From individuals to aggregations: the interplay between behavior and physics. J. Theoret. Bio. **196**, 397–454 (1999)
12. Fong, D., Geyer, W., Signell, R.: The wind-forced response on a buoyant coastal current: observations of the western Gulf of Maine plume. J. Mar. Sys. **12**, 69–81 (1997)
13. Franks, P.J.S.: Sink or swim: accumulation of biomass at fronts. Mar. Ecol. Prog. Ser. **82**, 1–12 (1992)
14. Franks, P.J.S.: Spatial patterns in dense algal blooms. Limnol. Oceanogr. **42**, 1297–1305 (1997)
15. Genin, A., Jaffe, J.S., Reef, R., Ricther, C., Franks, P.J.S.: Swimming against the flow: a mechanism of zooplankton aggregation. Science **308**(860), 4 (2005)
16. Helfrich, K., Pineda, J.: Accumulation of particles in propagating fronts. Limnol. Oceanogr. **48**, 1509–1520 (2003)
17. Lamb, H.: Hydrodynamics, 6th edn. Camb. Univ. Press, Camb., Eng. p. 738. (Dover edition, Dover publ., NY). See Ch. 1, Art. 14 (1932)
18. Nøttestad, L., Simlä, T.: Killer whales attacking schooling fish: why force a herring from deep water to the surface? Mar. Mamm. Sci. **17**(2), 343–352 (2001)
19. Olson, D.B., Backus, R.H.: The concentrating of organisms at fronts: a cold-water fish and a warm-core gulf stream ring. J. Mar. Res. **43**(1), 113–137 (1985)
20. Ostrand, W.D., Howlin, S., Gotthardt, T.A.: Fish school selection by marbled murrelets in Prince William Sound, Alaska: responses to changes in availability. Mar. Ornithol. **32**, 69–76 (2004)
21. Pedlosky, J.: Geophysical Fluid Dynamics, 2nd edn, p. 710. Springer, Berlin (1987)
22. Pitcher, K.W., Calkins, D.G.: Reproductive biology of steller sea lions in the Gulf of Alaska. J. Mammal. **62**, 599–605 (1981)

23. Rhines, P.B., Young, W.R.: How rapidly is a passive scalar mixed within closed streamlines? J. Fluid Mech. **133**, 133–145 (1983)
24. Rothschild, B.J., Osborn, T.R.: Small-scale turbulence and plankton contact rates. J. Plankton Res. **10**, 465–474 (1988)
25. Schoenherr, J.R.: Blue whales feeding on high concentrations of euphausiids around Monterey submarine canyon. Can. J. Zool. **69**(3), 583–594 (1991)
26. Sims, D.W., Quayle, V.A.: Selective foraging behaviour of basking sharks on zooplankton in a small-scale front. Nature **393**(6684), 460–464 (1998)
27. Werner, S., Beardsley, R., Lentz, S., Hebert, D., Oakey, N.: Observations and modeling of the tidal bottom boundary layer on the southern flank of Georges Bank. J. Geophys. Res. **108**(C11), 8005 (2003)
28. Wishner, K.F., Schoenherr, J.R., Beardsley, R., Chen, C.: Abundance, distribution and population structure of the copepod Calanus finmarchicus in a springtime right whale feeding area in the southwestern Gulf of Maine. Cont. Shelf Res. **15**, 475–507 (1995)
29. Woods, N.W.: Physical controls on copepod aggregations in the Gulf of Maine. Ph.D. thesis, MIT-WHOI Joint Program, p. 213 (2013)
30. Yen, J., Weissburg, M.J., Doall, M.H.: The fluid physics of signal perception by mate-tracking copepods. Phil. Trans. Roy. Soc. B **353**, 787–804 (1998)